Manuscript submitted to Tektonika

Preprint title:

Simultaneous deformation along the Main Ethiopian Rift and associated transversal lineaments: an analogue modelling perspective

Author names & email addresses:

Frank Zwaan[1,2] (frank.zwaan@gfz-potsdam.de) - Corresponding author (Twitter: @geozwaan)

Ameha A. Muluneh[1,3] (ameha@gfz-potsdam.de)

Jun Liu[1] (junliu@gfz-potsdam.de)

Ehsan Khosari[1] (ehsan@gfz-potsdam.de)

Matthias Rosenau[1] (rosen@gfz-potsdam.de)

Giacomo Corti[4] (giacomo.corti@igg.cnr.it) - (Twitter: @giacomo_corti)

Federico Sani[5] (federico.sani@unifi.it)

Author affiliations:

[1] Helmholtz Centre Potsdam - GFZ German Research Centre for Geosciences, Potsdam, Germany

[2] University of Fribourg, Department of Geosciences, Fribourg, Switzerland

[3] MARUM, University of Bremen, Germany

[4] CNR-IGG, Consiglio Nazionale delle Ricerche, Istituto di Geoscienze e Georisorse, Firenze, Italy

[5] Università di Firenze, Dipartimento di Scienze della Terra, Firenze, Italy

Simultaneous deformation along the Main Ethiopian Rift and associated transversal lineaments: an analogue modelling perspective

F. Zwaan[1,2*], A. A. Muluneh[1,3], J. Liu[1], E. Khosari[1], M. Rosenau[1], G. Corti[4] and F. Sani[5]

[1]*Helmholtz Centre Potsdam - GFZ German Research Centre for Geosciences, Telegrafenberg, 14473 Potsdam, Germany*

[2] *University of Fribourg, Department of Geosciences, Chemin du Musée 6, 1700 Fribourg, Switzerland*

[3] *MARUM, University of Bremen, Leobener Staße 8, 28359 Bremen, Germany*

[4] *CNR-IGG, Consiglio Nazionale delle Ricerche, Istituto di Geoscienze e Georisorse, Via G. La Pira 4, 50121 Firenze, Italy*

[5] *Università di Firenze, Dipartimento di Scienze della Terra, Via G. La Pira 4, 50121 Firenze, Italy*

**Corresponding author (e-mail: frank.zwaan@gfz-potsdam.de)*

Abstract

The interaction between the NE-SW striking Main Ethiopian Rift (MER) and the E-W oriented Yerrer-Tullu Wellel Volcano-tectonic lineament (YTVL) represents one of the least understood tectonic problems in the East African Rift System. Despite the numerous studies that have been conducted in the region, the following questions still remain to be answered: did the MER and YTVL evolve simultaneously? Was there a stress reorientation to allow a diachronous evolution of the rift and the lineament? How does the E-W oriented YTVL remain active under an E-W oriented stress field? Previous studies propose a two-phase tectonic evolution, involving a stress reorientation at around 6 Ma causing deformation to focus in the MER. However, this interpretation contradicts plate-tectonic reconstruction data suggesting a constant plate divergence direction since ca. 16 Ma. We use analogue models to study how deformation may occur along the YTVL. We find that the activation of lineaments oriented (near-)parallel to the plate divergence direction is in fact possible, if (1) the weakness sufficiently reduced the strength of the crust and (2) the main rift trend is sufficiently oblique to the plate divergence direction. As such, no multiphase scenario is required to explain the development of the YTVL, and a single-phase scenario that is in line with plate tectonic reconstructions can be adopted instead. Moreover, our model results suggest that also other lineaments associated with the MER could be active in the current tectonic regime. These insights may be of relevance to the interpretation of similar structures in rift systems around the world as well.

1. Introduction

The Main Ethiopian Rift (MER) forms the northern section of the East African Rift System (EARS) and connects the Afar depression in the north, where the EARS links with the Red Sea and Gulf of Aden Rifts, to the Turkana depression in the south (Fig. 1, e.g., Corti, 2009). The MER is a narrow rift valley that accommodates the active extensional deformation between the diverging Nubia and Somalia Plates (e.g., Michon et al., 2022). Nubia-Somalia divergence currently occurs in a roughly E-W direction at rates of ~4-6 mm/yr (e.g., Saria et al., 2014; Stamps et al., 2021), and plate kinematic models suggest this motion has been constant (in terms of plate divergence direction) over the last 16-17 Myr (DeMets and Merkouriev, 2021).

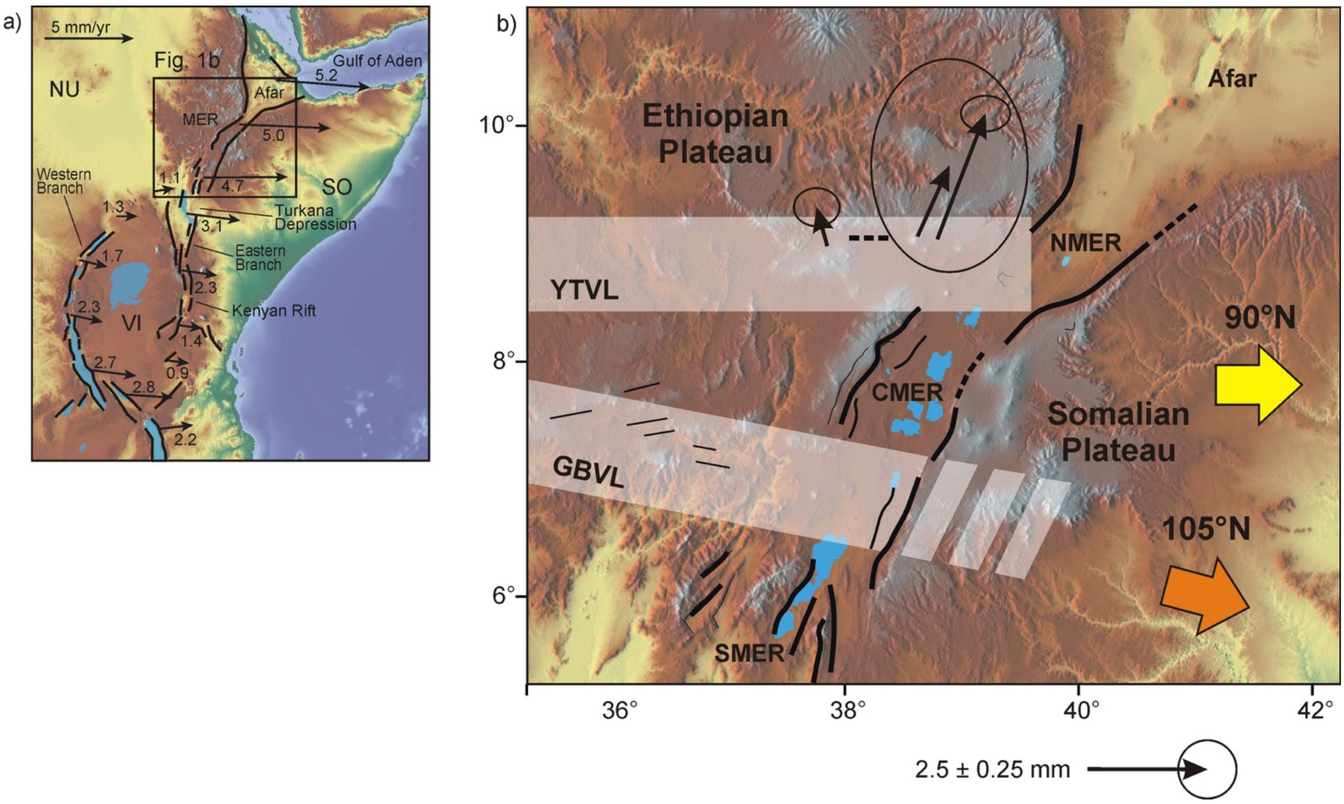

Fig. 1. a) Location of the Main Ethiopian Rift (MER) as the northern part of the East African Rift System, which splits the African continent in the Nubian Plate (NU) to the west and the Somalian Plate (SO) to the east (with the Victoria Microplate [VI] in between). GPS-based plate displacement after Saria et al. (2014). b). Distribution of the subsections of the Main Ethiopian Rift and the associated volcanotectonic lineaments. The yellow and orange arrows indicate the range of plate divergence direction, i.e., E-W (90˚N) and WNW-ESE (105˚N), respectively. Active displacement along the YTVL is indicated with GPS vectors adopted from Knappe et al. (2020). NMER: Northern MER, CMER: Central MER, SMER: Southern MER, YTVL: Yerer-Tullu Wellel Volcano-tectonic Lineament, GBVL: Goba-Bonga Volcano-tectonic lineament. Images Modified after Keranen & Klemperer (2008) and Corti et al. (2018).

The MER is generally considered to consist of three different domains (Northern MER; Central MER and Southern MER; Fig. 1), which differ in terms of orientation, fault pattern, crustal/lithospheric characteristics, age of onset of rifting and volcanism (e.g., Corti, 2009). The fault pattern is dominated in the different rift segments by large boundary faults separating the rift floor from the surrounding plateaus: the trend of these faults varies from ~N-S in the south to ~45° in the north (e.g., Agostini et al., 2011). In the southern and central MER, the boundary faults accommodate rifting with subordinate activity of the rift floor faults (Corti et al., 2020). In contrast, in the northern MER, more than 50% of the rift opening is accommodated in ~20 km wide, 60 km long magmatic segments (Wolfenden et al., 2004). These along-axis variations in deformation style have been interpreted to reflect different stages of rifting, from initial rifting dominated by faulting in the Southern MER break-up in the Northern MER, dominated magmatism along the rift axis (e.g., Hayward and Ebinger, 1996).

The transition between the different MER segments is defined by major structures (lineaments) transverse to the rift trend, extending hundreds of kilometres away from the margins of the MER, mainly on the Ethiopian Plateau, but also on the Somalian Plateau (e.g., Abebe Adhana, 2014) (Fig. 1). The Yerer-Tullu Wellel Volcano-tectonic Lineament (YTVL; e.g., Abebe et al., 1998), which extends for some 700 km from the western margin of the MER to Tullu Wellel near the border with Sudan, is the most important of these transverse structures (Fig. 1). The YTVL separates the Northern MER, where the undeformed crust of the plateau is ca. 50 km thick, from the Central MER, where the crust is ca. 40 km thick (Fig. 1; Keranen et al., 2009). The YTVL forms a tectono-magmatic system characterized by a roughly E-W alignment of normal faults and major volcanic centers (e.g., Abebe et al., 1998; Tommasini et al., 2005; Abebe Adhana, 2014). Seismicity and geodetic data show that the YTVL is experiencing ongoing deformation, with increasing surface displacement towards the east, i.e. towards the MER (Keir et al., 2006, 2009; Knappe et al., 2020). The second major E-W-trending transverse lineament is the Goba-Bonga Volcano-tectonic lineament (GBVL; e.g., Merla et al., 1979; Abbate and Sagri, 1980; Corti et al., 2018), which marks the boundary between the Central MER and the Southern MER (Fig. 1).

Both the YTVL and GBVL have likely been controlled by pre-existing Neoproterozoic weaknesses sub-parallel to the trend of the Gulf of Aden in the north, and transversal to the MER rift valley (e.g., Abebe et al., 1998; Korme et al., 2004; Abbate and Sagri, 1980; Abebe Adhana, 2014; Corti et al., 2018, 2022). This interpretation is supported by geophysical data imaging a significant crustal thickness contrast in correspondence to the YTVL (Keranen and Klemperer, 2008) and thermal anomalies and localized lithosperic thinning beneath this transveral lineament (Bastow et al. 2008), likely caused by inheritance in the form of either inherited lithospheric thinning, or by syn-rift extension exploiting pre-rift weakness zones (Corti et al., 2022).

Given that the orientation of these transversal lineaments is subparallel to the plate divergence, their activation and role in development of the MER remains to be clarified. Keranen and Klemperer (2008) have suggested a two-phase rifting scenario, with an initial (Miocene) stage of rift development primarily controlled by lithospheric structures under a 130°N oriented plate divergence and a later (Pliocene-recent) phase of 105°N oriented plate divergence during which magmatic processes dominated. In the initial phase, rifting-related deformation would have been diverted away from the modern rift valley, resulting in the activation of the YTVL; in the later phase, extensional deformation would have localized within the current rift valley to form the central MER. Modeling works (e.g., Erbello et al., 2016; Corti, 2008) and plate kinematics analysis (e.g., DeMets and Merkouriev, 2016; 2021) argue against such a two-phase evolution, suggesting that MER rift kinematics have remained constant (under E-W [90˚N] to ESE-WNW [105˚N] plate divergence) from Miocene times on. However, also if rift kinematics have remained constant, the ongoing deformation along the YTVL (Keir et al., 2006, 2009; Knappe et al., 2020) remains controversial, since its E-W orientation should be unfavourable for localizing deformation (e.g., Zwaan & Schreurs, 2017; Bonini et al., 2023; Zou et al., 2023). The same goes for any potential ongoing deformation along the GBVL.

Analogue tectonic modelling provides an excellent tool to test the dynamic evolution of rift systems, and many previous modelling studies analyzed the activation of structural weaknesses during single- and multiphase rifting (e.g., Henza et al., 2010, 2011; Zwaan et al., 2021; 2022; Wang et al., 2021; Bonini et al., 2023; Zou et al., 2023). Nevertheless, despite these previous works, conclusive insights on how contemporaneous strain localization occurs along the structural lineaments in the MER, which are oriented sub-parallel to the divergence direction, are still lacking. In this paper we use analogue models that are specifically designed to replicate the situation in the MER to study how deformation may occur along the structural lineaments oblique to the MER. Using these model results, we see how lineaments striking (near-)parallel to the plate divergence can in fact be activated during a single phase of rifting. As such, the multiphase deformation scenario proposed by Keranen & Klemperer (2008) is not required for the active deformation that is currently observed along the YTVL (and GBVL). Instead, a simpler single-phase scenario that is more in line with plate tectonic reconstructions can be adopt

2. Methods

2.1. Materials

In our models, we use both frictional and viscous materials to simulate brittle and ductile layers of the continental crust. A 3 cm thick layer of G12 quartz sand, which has a grain size range of 100-400 μm, an internal peak friction angle of 35˚, a sieved density of 1700 kg/m^3, and a cohesion of 50-110 Pa (Table 1, Rosenau et al., 2018), serves to represent a 22.5 km thick brittle upper crust. Below this sand layer, a 1 cm thick layer of viscous material simulates a 7.5 km thick ductile lower crust. This near-Newtonian viscous material is a mixture of G20OH polydimethylsiloxane (PDMS) and fine NKF120 Corundum sand, with a density of ca. 1600 kg/m^3 and a viscosity of $1·10^5$ Pa·s (Table 1). Details on scaling are provided in the Appendix and Table A1.

2.1. General model set-up

Our model set-up, which is inspired by the one applied by Zwaan et al. (2021, 2022), involves a base plate placed below the two layers of model materials representing the upper and lower continental crust (Fig. 2a). The base plate is pulled by precise computer-controlled stepper motors, moving it away from under the model materials so that the edge of the plate creates a velocity discontinuity (VD). This VD induced deformation in the overlying model materials, thus creating a rift structure along its length (e.g., Tron & Brun, 1991; Brun & Tron, 1993; Bonini et al., 1997; Keep & McClay, 1997; Michon & Merle, 2000; Zwaan et al., 2019; Bonini et al., 2023), which can be considered analogous to the Main Ethiopian Rift in nature. Moreover, in order to simulate lineaments such as the YTVL and GBVL, we added "seeds", i.e. semi-circular ridges of viscous material on top of the viscous layer (Fig. 2a). By doing so, we locally reduced the integrated strength of the sand layer, which leads to localization of deformation, apart from the deformation controlled by the VD (e.g., Zwaan et al., 2021; 2022). In our models, this seed is intended to represent the inherited weakness caused by the difference between the crust to the north and south of the YTVL (Keranen et al., 2009, Fig. 1). The 50 cm wide, 50 cm long and 4 cm high models were contained by sand taluses on each side, to prevent viscous materials from flowing out from below the overlying sand layer (Fig. 2a).

Table 1. Model material properties

Granular materials	Quartz sand G12 [a]	Corundum sand NKF120[b]
Grain size range (ø)	100-400 μm	90-120 μm
Specific density ($\rho_{specific}$)[c]	2650 kg/m^3	4000 kg/m^3
Sieved density (ρ_{sieved})	1700 kg/m^3	2240 kg/m^3
Angle of internal peak friction (φ_{peak})	35˚	37˚
Coefficient of internal peak friction (μ_{peak})[d]	0.69	0.75
Angle of dynamic-stable friction (φ_{dyn})	29˚	30˚
Coefficient of dynamic-stable friction (μ_{dyn})[d]	0.55	0.57
Angle of reactivation friction (φ_{react})	32˚	32˚
Coefficient of reactivation friction (μ_{react})[d]	0.62	0.62
Cohesion (C)	50-110 Pa	100-150 Pa
Viscous materials	**PDMS (G20OH)[c]**	**PDMS/corundum sand mixture[d]**
Weight ratio PDMS : corundum sand	-	1:1
Density (ρ)	970 kg/m^3	ca. 1600 kg/m^3
Viscosity (η)	ca. $2{\cdot}10^4$ Pa·s	ca. $1{\cdot}10^5$ Pa·s[f]
Rheology[f]	Newtonian (n = ca. 1)[g]	near-Newtonian (n = 1.05-1.10)[g]

[a] **Quartz sand properties after Rosenau et al. (2018).**

[b] **Corundum sand characteristics after Rosenau & Pohlenz 2023**

[c] **Pure PDMS rheology after Rudolf et al. (2016)**

[d] **PDMS-corundum mixture rheology after Zwaan et al. (2018)**

[e] **$\mu = \tan(\varphi)$**

[f] **Viscosity value holds for model strain rates ($< 10^{-4}$ s^{-1}) (Rudolf et al., 2016)**

[g] **Power-law exponent n (dimensionless) represents sensitivity to strain rate**

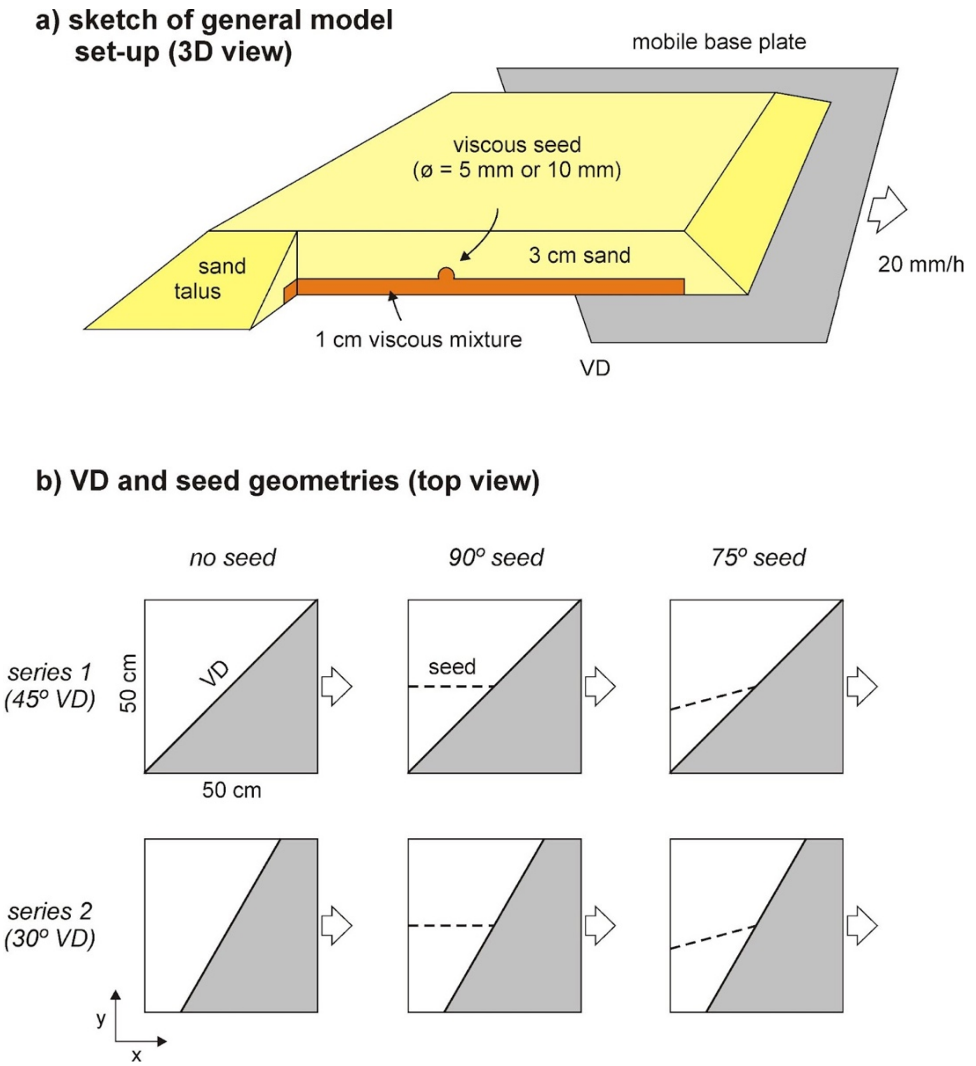

Fig. 2. Model set-up. (a) 3D sketch of model set-up and layering. (b) orientations of VD (velocity discontinuity) and seeds in the various models. The 45˚ oblique VD models of Series 1 represent an end-member situation with pure E-W (90˚N) divergence in the MER, whereas the 30˚ oblique VD represent an end-member situation with ca. WNW-ESE (105˚N) plate divergence in the MER. See also Table 2 for details on model parameters.

2.2. Model parameters

We present a total of 10 models, split in two series, which are aimed to test the reactivation of lineaments in the context of the YTVL and MER (Figs. 1, 2, Table 2). In the first series, we apply a 45˚ (measured in clockwise direction) oriented VD, which together with the 90˚ base plate motion direction would represent pure E-W (90˚N) tectonic plate divergence end member in nature, given the ca 45˚N orientation of the (Northern) MER (Fig. 1). In the second series, we apply a 30˚ oriented VD, which in combination with the 90˚ base plate motion would represent a 105˚E plate divergence direction end member in nature (Fig. 3). Moreover, both series contained a reference model without seed, as well as four models including seeds each. In these latter models, we vary the orientation of the seeds to explore the impact of pre-existing weakness orientation on lineament (re)activation. In addition, we vary the diameter of the seed (either 5 or 10 mm) to explore the impact of the relative weakness of structural inheritance on lineament (re)activation. In all models, the divergence velocity is 20 mm/h, translating to the 5 mm/yr as observed in the present-day MER (e.g., Saria et al., 2014) (see the Appendix for details on scaling). The full model run duration is 90 min, amounting to a total of 30 mm of divergence.

Table 2. Overview of model parameters

	Model name	**VD (simulated MER) orientation***	**Seed (simulated tectonic lineament) orientation**	**Seed diameter**
Series 1	R1	45˚	-	-
	A1	45˚	90˚	5 mm
	A2	45˚	90˚	10 mm
	A3	45˚	75˚	5 mm
	A4	45˚	75˚	10 mm
Series 2	R2	30˚	-	-
	B1	30˚	90˚	5 mm
	B2	30˚	90˚	10 mm
	B3	30˚	75˚	5 mm
	B4	30˚	75˚	10 mm

*** VD: velocity discontinuity, MER: Main Ethiopian Rift. See Figs. 1 and 2 for tectonic context and model set-up, respectively.**

2.3. Model analysis

We use a digital image correlation technique (particle image velocimetry, PIV) for quantitative surface deformation monitoring (e.g., Adam et al., 2005). A stereoscopic pair of two 12-bit, 29-megapixel monochrome cameras (LaVision Imager XLite 29M) is deployed to monitor surface deformation at high spatial (8 px/mm) and temporal resolution. One image is taken every 0.5 mm of displacement. Recorded image sequences are processed by commercial PIV software LaVision Davis 10.1 to derive the surface topography and the three-dimensional surface velocity (or incremental displacement) field, from which any component of the 3D surface incremental and cumulative strain tensor can be derived. To exclude boundary effects, we choose a central area of interest. The spatial resolution of the processed vector fields is 2 mm in terms of grid cell size and <5 μm in terms of displacement precision. For visualization and analysis of the surface deformation, we trace model topography and horizontal displacement over time. Moreover, we map the incremental horizontal maximum normal (or principal) strain as an absolute measure of strain.

3. Results

3.1. Series 1 model results

An overview of the results of the Series 1 models, all with a 45˚ VD orientation representing 90˚N (E-W) plate divergence in nature (Fig. 1, 2b), is provided in Fig. 3. Reference model R1 shows the impact of the 45˚oblique VD without the presence of a seed (Fig. 3a-d). Deformation along the VD creates a ca. 6.5 cm wide graben that is bounded by both VD-parallel normal faults and a series of en echelon normal faults with a counterclockwise deviation in strike of ca. 20˚ with respect to the main graben trend. The displacement field shows how material above the mobile plate is displaced to the side, at the same rate as the plate. In the graben along the VD, this displacement is reduced, whereas minor displacement is registered on the graben shoulders opposite side. Velocities decrease stepwise across the graben structure from plate velocity in the model E to zero in the model W. Steps in the velocity field correspond to faults. A very similar situation occurs in Model A1, which has a 90˚ seed with a diameter of 5 mm that does not activate (Fig. 3e-h).

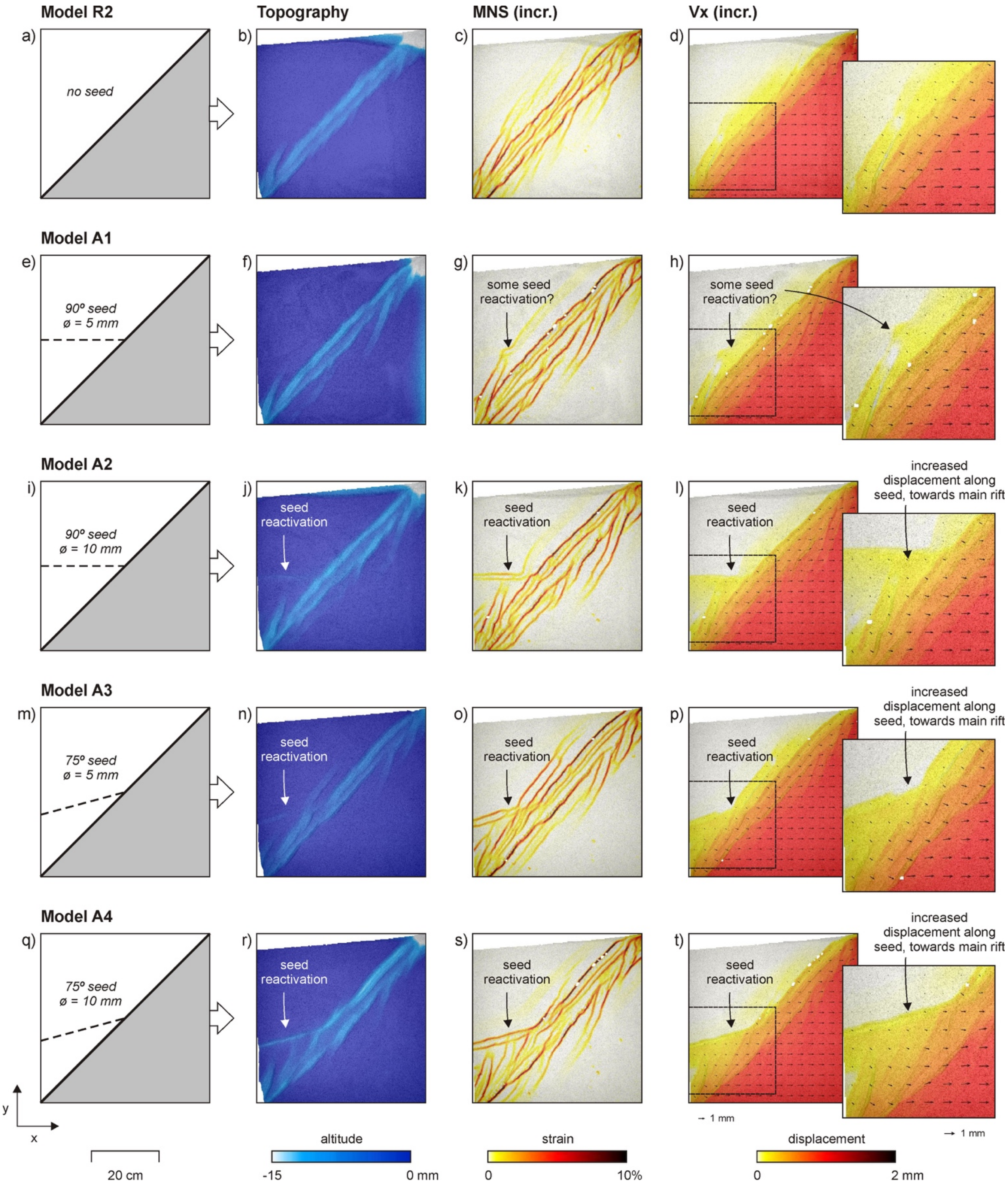

Fig. 3. Overview of model results from Series 1 at t = 90 min (base plate divergence = 30 mm), showing topography, incremental maximum normal strain (MNS, used as a proxy for active faulting), and displacement in the x-direction (i.e., the base plate motion direction). Vectors in the Vx maps indicate the full incremental displacement direction and magnitude. Incremental data are computed over a 1 mm base plate divergence interval.

By contrast, when increasing the diameter of the seed to 10 mm in Model A2, minor deformation is localized along the seed (Fig. 3i-l). This localization of deformation is associated with additional displacement between the seed and the main graben (Fig. 3l). Moreover, applying a 75˚ seed orientation in Model A3 allows a 5 mm diameter seed to be activated (Fig. 3m-p), whereas a 10 mm seed in Model A4 causes significant localization of deformation (Fig. q-t), as best illustrated by the final model topography results (Fig. 3r). In both cases, we observe additional displacement between seed and main graben. However, it may be noted that in all models that involve localization of deformation along the seeds, the structure of the main graben remains very similar (Fig. 3i-t). Moreover, in all models that show the activation of a seed, we observe a gradual increase of opening towards the main graben, when moving along the seed (insets in Fig. 3l, p, t).

3.2. Series 2 model results

An overview of the results of our Series 2 models, all with a 30˚ VD orientation that represents 105˚N (roughly WNW-ESE) plate divergence in nature (Figs. 1, 2), are provided in Fig. 4. Reference Model R2 illustrates the impact of the 30˚ oblique VD without a seed being present (Fig. 4a-d). Similar to Model R1, we obtain a graben structure along the VD, including en echelon boundary faults that are striking ca. 15˚ counterclockwise from the main graben. However, the graben itself is significantly wider in Model R2 than in Model R1 (7.5 cm vs. 6.5 cm, respectively). The displacement field also shows how material on top of the mobile plate is moving at the same rate as the plate, whereas this displacement is reduced in the graben, and minor displacement is recorded on the opposite graben shoulder (Fig. 4d). The same result is obtained with Model B1, which contains a 5 mm thick seed that is oriented 90˚ and does not activate (similar to the same seed in Model A1) (Fig. 4e-h).

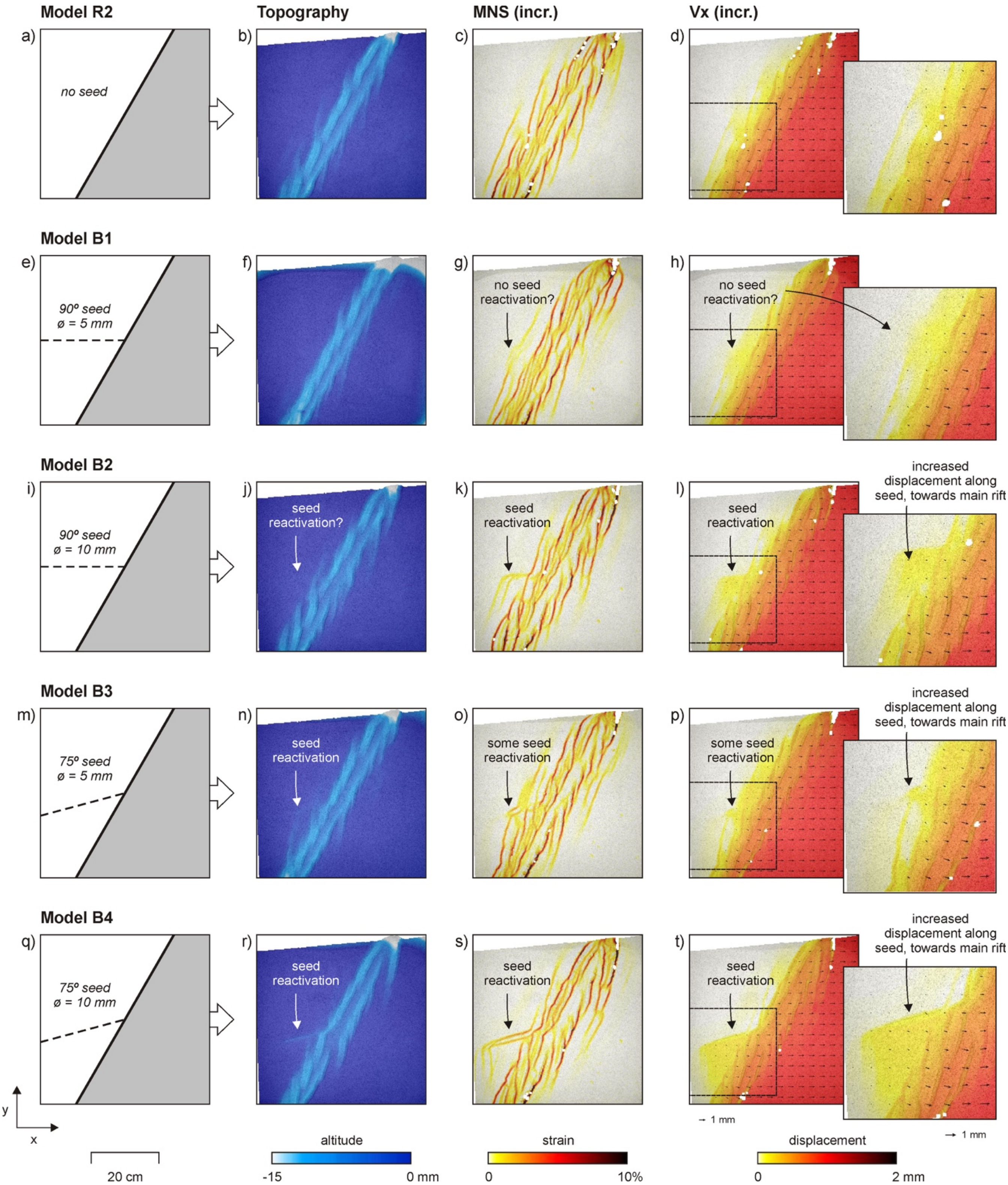

Fig. 4. Overview of model results from Series 2 at t = 90 min (base plate divergence = 30 mm), showing topography, incremental maximum normal strain (MNS, used as a proxy for active faulting), and displacement in the x-direction (i.e., the base plate motion direction). Vectors in the Vx maps indicate the full incremental displacement direction and magnitude. Incremental data are computed over a 1 mm base plate divergence interval.

We do observe minor reactivation of the thicker (10 mm) seed in Model B2 (Fig. 4i-l). When the 5 mm thick seed is oriented 75˚ in Model B3, we get slightly more localization of deformation (Fig. 4m-p), but only when the seed diameter is increased to 10 mm in Model B4, we observe significant activation, similar to that in the Series 1 models (Figs. 3, 4q-t). In the cases where the seed is activated, we observe increased displacement between the seed and main graben, and a similar gradual increase of deformation towards the graben as in the Series 1 models (Figs. 3l, p, q, 4l, p, q). Yet it is clear that the impact of the seed on the surface structures in the Series 2 models is significantly reduced with respect to their equivalents in series 1 (Figs. 3, 4). Finally, in all Series 2 models, the main graben structure is very similar.

3.3. Detailed analysis of models A2 and B4

We provide a more detailed analysis of Models A2 and B4, which we consider key models since they may best represent the situation in the MER (see section 4.2).

The evolution of Model A2, with a 45˚ VD orientation and a 90˚ striking seed of 10 mm diameter that would represent a 90˚N (pure E-W) divergence setting in nature, is shown in Fig. 5. We observe the gradual development of the main graben as it grows in both depth and width, as indicated by the topography evolution and the active fault patterns (Fig. 5a-f). However, the active faulting and displacement data show how the seed localizes deformation from the earliest stages of the model run on (Fig. 5d-i). Also the gradient towards the main graben is established early on (Fig. 5g-i).

We show the evolution of Model B4, with a 30˚ VD orientation and a 75˚ striking seed of 10 mm diameter representing a 105˚N (roughly WNW-ESE) divergence scenario in nature, in Fig. 6. Similar to Model B4, the topography results and active faults show a gradual development of the main graben (Fig. 6a-f), whereas the active faulting and displacement data show a similar activation of the seed since the early stages of the deformation (Fig. 5d-i). Moreover, the gradient towards the main graben is established early on in Model B4 too (Fig. inset 6g-i).

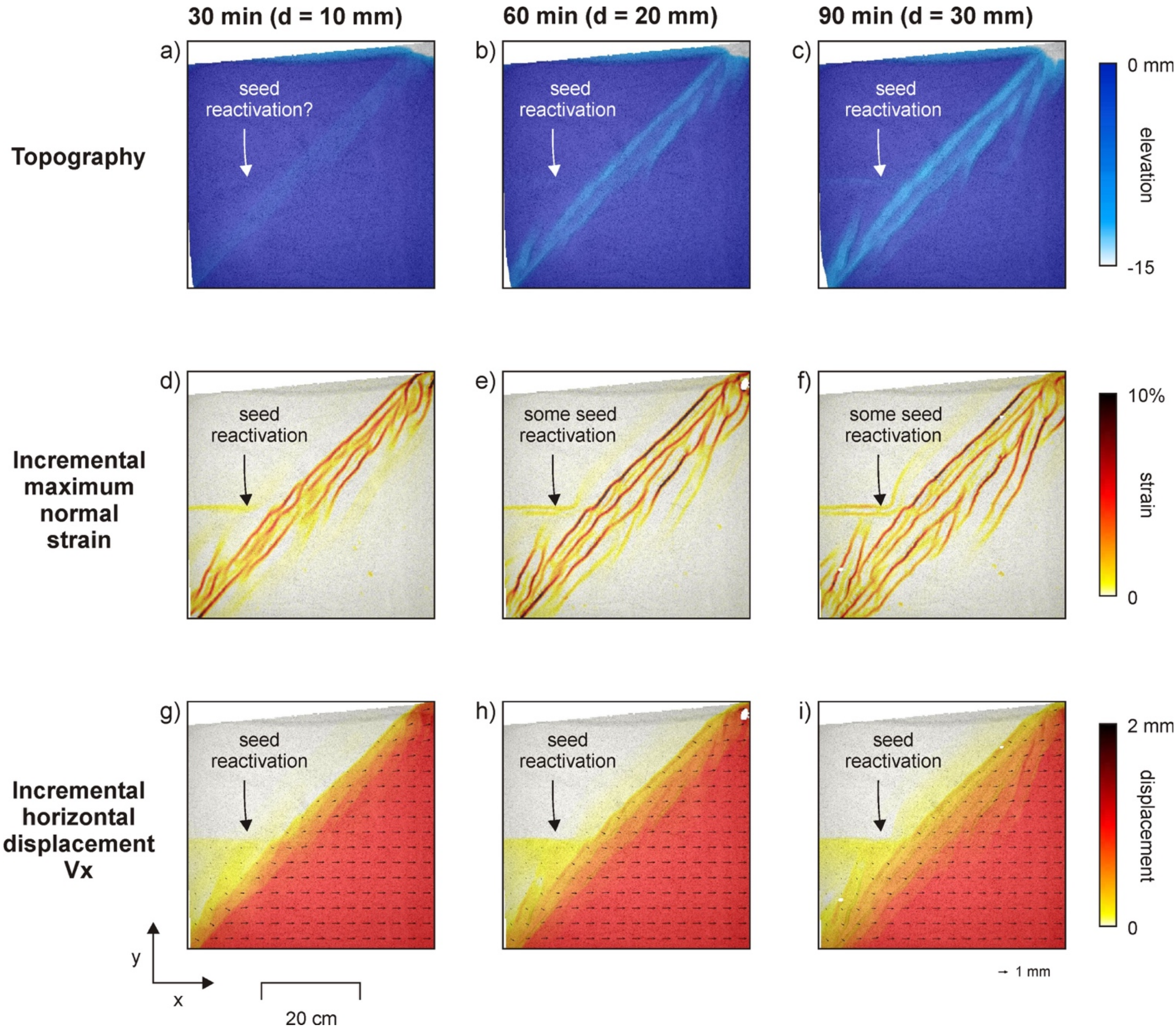

Fig. 5. Evolution of key Model A2 from Series 1 (45˚ VD and a 10 mm thick seed with a 90˚ orientation, representing the ca. E-W [90˚N] plate divergence end-member in the Main Ethiopian Rift). Topography data are incremental, maximum normal strain and Vx-displacement data are incremental (computed over a 1 mm base plate divergence interval). Vectors in (g-i) indicate the full incremental displacement direction and magnitude.

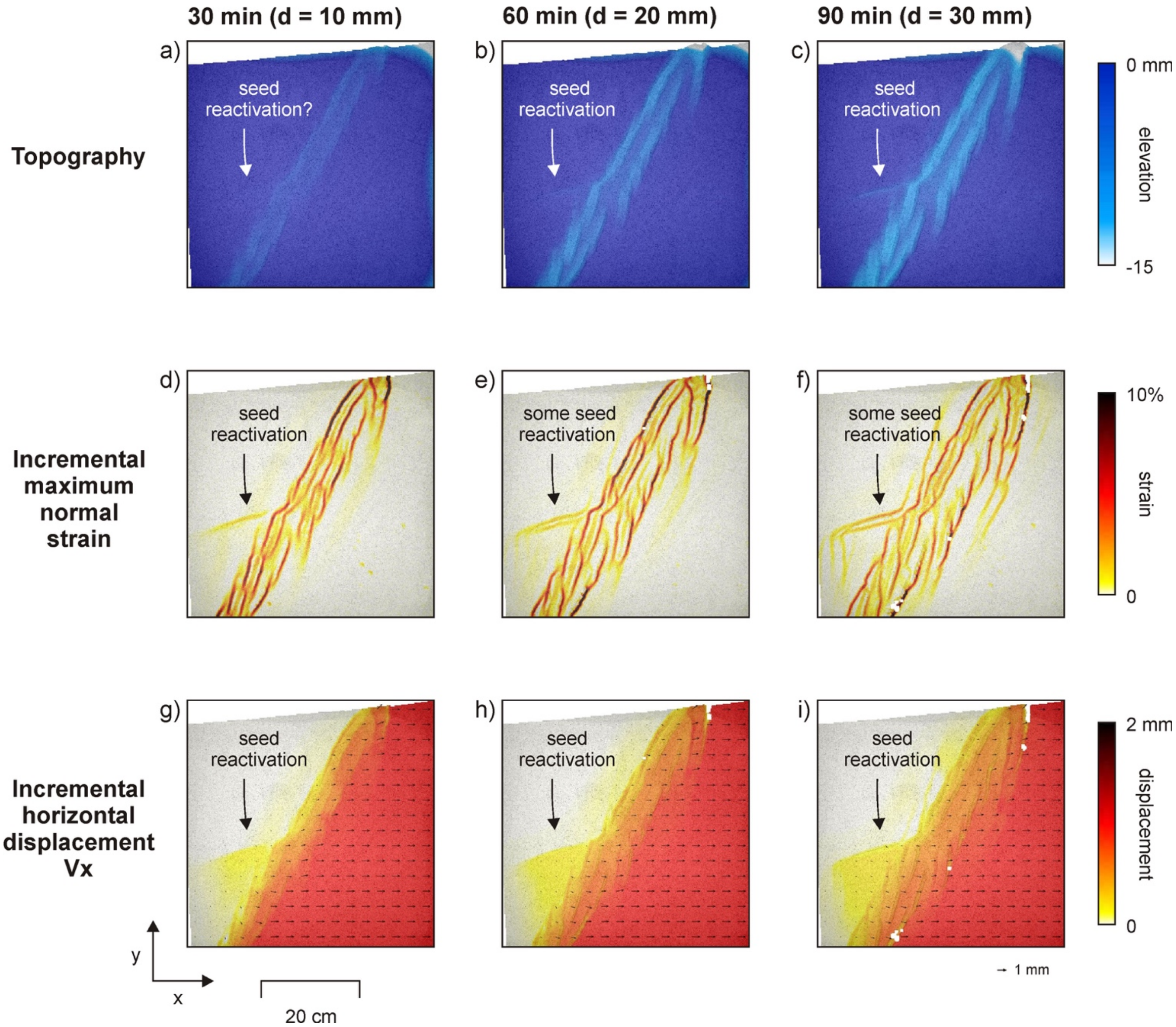

Fig. 6. Evolution of key Model B4 from Series 2 (30˚ VD orientation and a 10 mm thick seed with a 90˚ orientation, representing the ca. WNW-ESE [105˚N] plate divergence end-member in the Main Ethiopian Rift). Topography data are incremental, maximum normal strain and Vx-displacement data are incremental (computed over a 1 mm base plate divergence interval). Vectors in (g-i) indicate the full incremental displacement direction and magnitude.

4. Discussion

4.1. Interpretation of model results and comparison with previous works

Our model set-up is tailored to the situation in the MER, but the results are very much in line with previously published modelling studies, as summarized in Fig. 7. The en echelon structures we observe in both reference models (R1 and R2) are characteristic of oblique rifting models (e.g., Withjack & Jamison 1986; Tron & Brun 1991; Keep & McClay 1997; Bonini et al., 1997; Agostini et al., 2009; Zwaan et al., 2022) (Fig. 7a, b). Also the use of seeds as structural weaknesses has a clear precedent (e.g., Le Calvez et al., 2002; Zwaan & Schreurs 2017; Molnar et al., 2019, 2020; Zwaan et al., 2021, 2022). The relative impact of such weaknesses, i.e., their activation as a function of the degree to which they locally reduce the strength of the brittle (sand) layer (in this study controlled by the diameter of the seed, Fig. 7c, d) fits with observations from previous works as well (Osagiede et al., 2021; Zwaan et al., 2021; Bonini et al., 2023). Moreover, we find that the orientation of the (crustal) weakness is of great importance for its activation (Fig. e, f); weaknesses that are oriented near-orthogonal to the divergence direction tend to activate much better than those oriented oblique to the divergence direction, as observed in Zwaan et al. (2021, 2022), Bonini et al. (2023), and Zou et al. (2023).

Even so, we do see the activation of seeds that are parallel to the divergence direction in our models with oblique rifts (Fig. 7c-h), which is in contrast to previous modelling works in which such activation of crustal weaknesses is not observed (e.g., Zwaan & Schreurs 2017; Corti et al., 2018; Zou et al., 2023). It seems that the oblique main graben arrangement in our present study may induce some reorientation of stresses at its margins, thus allowing for activation of these otherwise unfavourably oriented seeds. This interpretation is supported by the impact of the VD orientation: in the 30˚ VD (Series 2) models, the seeds localize less deformation than in the 45˚ (Series 1) models (Fig. 7g, h). This is most likely due to the VD in the Series 1 models being less well oriented for localizing deformation than in the Series 2 models (the ideal VD orientation being 0˚), allowing more opportunity for the seed to attract deformation instead. Similar interplay between seeds and the VD with different orientations is also observed in Zwaan et al. (2021, 2022).

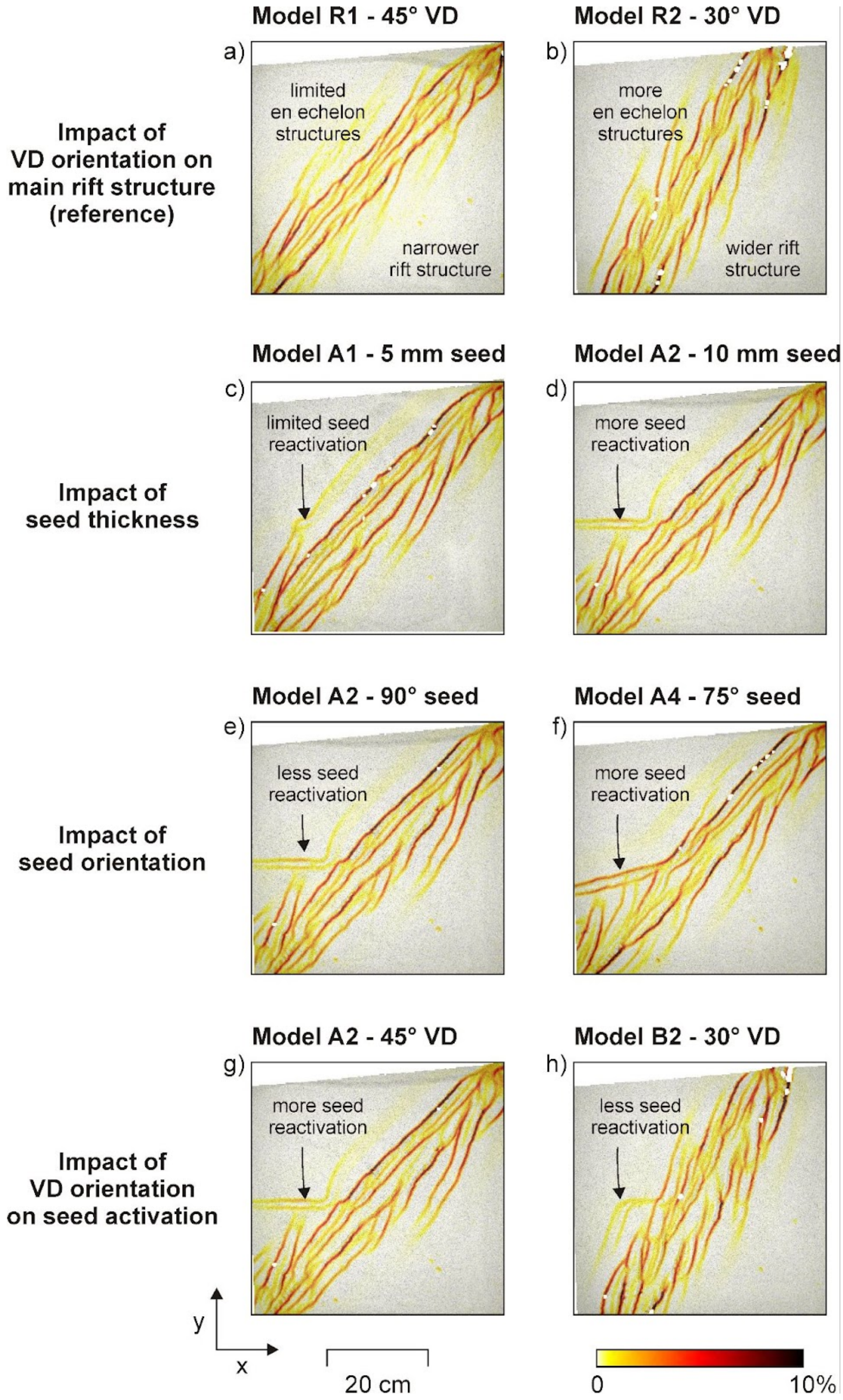

Fig. 7. Summary highlighting the impact of the various parameters tested on tectonic lineament activation. The top view incremental maximum normal strain (MNS) images depict the situation at the end of the model run (i.e., after 90 min, or 30 mm of divergence).

Before moving to an application of our model results to interpret the situation in the MER, we should point out a couple of limitations to our crustal scale modelling approach. We do not include magmatism that is widespread in the MER, nor do we apply surface processes or lithospheric-scale isostasy. The exclusion of magmatism is however permissible, since we are focussing on the development of the YTVL, which is a lineament outside of the magma-rich MER. Moreover, the YTVL is characterized by a limited, mostly inactive volcanism (Abebe et al., 1998); therefore, the contribution of magmatic processes to its development and evolution is negligible. The omission of both surface processes and isostasy is reasonable due to the limited impact these processes are expected to have on the large-scale structural arrangement and general tectonic evolution of early-stage rift systems such as the MER (Zwaan et al., 2018). Despite those limitations, our modelling work captures the main tectonic characteristics of the MER and its transversal lineaments.

4.2. Interpretation of model results and comparison with previous works

Several scenarios have been proposed to explain the development of the MER and the YTVL. Keranen and Klemperer (2008) propose that deformation along the YTVL ceased since ~2 Ma (Pliocene-recent), due to a rotation of the regional stress field linked to a shift in plate kinematics. However, this polyphase tectonic model has been questioned by several modelling and field observations that suggest that the current plate motion along the MER has been constant since at least the mid-Miocene (e.g., DeMets and Merkouriev, 2021), while a constant opening direction of the MER best explains the basinward localization of deformation over the past 2 Myr (Corti, 2008; Erbello et al., 2016; Muluneh et al., 2020). Even so, insights from generic tectonic modelling studies suggest that the unfavourably oriented YTVL should not have been active under such E-W plate divergence. As such, a holistic scenario that convincingly explains the simultaneous deformation along the MER and YTVL has not been available so far.

Our novel analogue modelling study now enables us to propose such a scenario. When comparing our new model results to the situation in the MER, we find that both Model A2 and Model B4 (when rotated 15˚ clockwise) reproduce the first-order observations in nature (Fig. 8). In both models, the MER develops while the YTVL is activated as an extensional lineament, likely due to local stress changes linked to the interaction between the oblique MER and YTVL. Moreover, we observed an increase in deformation activity towards the modelled MER, as is also the case in nature (Keir et al., 2006, 2009; Knappe et al., 2020, Fig. 8). The simultaneous development of the MER and YTVL during a single continuous rifting phase, because of their particular orientation, is thus shown to have been possible without the need for the multiphase scenario put forward by Kernanen & Klemperer (2008). Moreover, as the GVBL has a very similar orientation with respect to the MER as does the YTVL, the tectonic arrangement would also have allowed for its activation during single-phase MER. Future GPS analysis and tectonic fieldwork may confirm this activity.

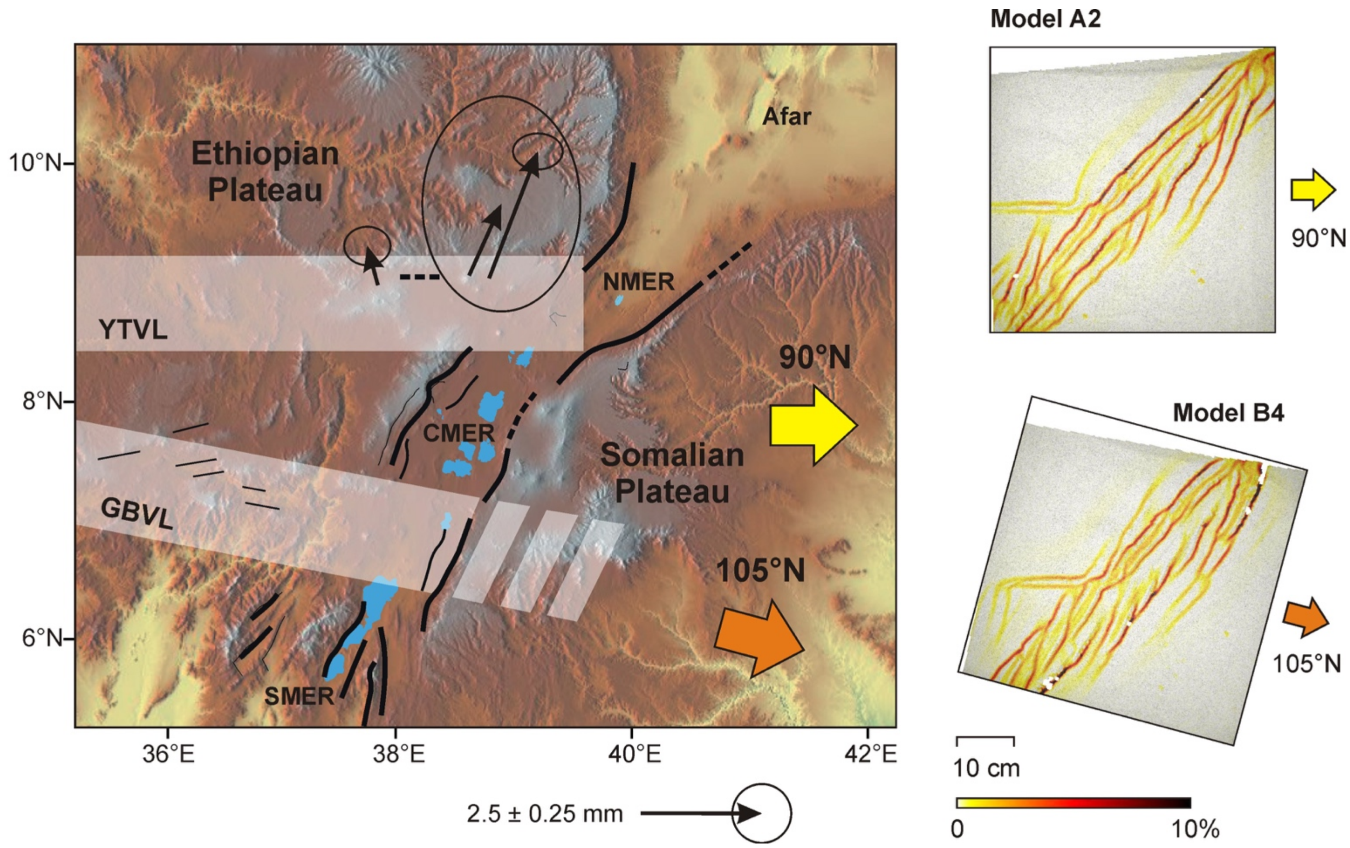

Fig. 8. Comparison between model results and natural situation in the Main Ethiopian Rift. The model A2 and B4 maximum normal strain (indicating active faulting) results at t = 90 min (30 mm or displacement) show a good fit, indicating that both 90˚N and 105˚N plate motion end members can allow for activation of the Yerer-Tullu Wellel Volcano-tectonic Lineament (YTVL). NMER: Northern MER, CMER: Central MER, SMER: Southern MER, GBVL: Goba-Bonga Volcano-tectonic lineament. Image modified after Keranen & Klemperer (2008) and Corti et al. (2018). Active displacement along the YTVL is indicated with GPS vectors adopted from Knappe et al. (2020).

5. Conclusion

We have conducted a series of analogue tectonic models that are specifically designed to replicate the situation in the Main Ethiopian Rift (MER), in order to study how deformation may localize along the structural lineaments associated to the rift, despite their highly unfavourable orientation with respect to the regional divergence direction. Our model results lead us to the following conclusions:

- Surprisingly, the activation of lineaments along weaknesses that are oriented (near-)parallel to the plate divergence direction is indeed possible, if (1) the weakness sufficiently reduced the strength of the crust to allow for deformation localization, and (2) the main rift trend is sufficiently oblique to the plate divergence direction, likely allowing for a local reorientation of extension leading to lineament activation, even if this lineament is unfavourably oriented.

- The multiphase deformation scenario for the MER- and Yerer-Tullu Wellel Volcano-tectonic Lineament (YTVL) evolution as proposed by Keranen & Klemperer (2008) is not required for development of the YTVL. Instead, our models show that a single-phase scenario, which is more in line with plate tectonic reconstructions, can be adopted.

- Similarly, we may expect active deformation along the Goba-Bonga Volcano-tectonic lineament (GVBL), which has a similar orientation as the YTVL, and a similar arrangement with respect to the MER.

The insights from our study, especially the observation that single-phase rifting can reactivate unfavourably aligned lineaments, may be of use beyond the MER as well, since many rift systems around the world involve weaknesses and lineaments that have reactivated, as well as various degrees of oblique divergence (e.g., Brune et al., 2018). Examples may be the various basins along the East African Rift System, the Red Sea and South Atlantic (see e.g., Molnar et al., 2019, 2020).

Acknowledgements

We thank Frank Neumann and Thomas Ziegenhagen for technical assistance in the lab, and Kirsten Elger and Florian Ott for helping us prepare a GFZ data publication containing the supplementary material (Zwaan et al., 2024). Frank Zwaan received financial support from the GFZ Discovery Fund, Ameha Muluneh has been funded by German Research Foundation (DFG, 537025018), Jun Liu received financial support from the China Scholarship Council (CSC NO. 202006190038).

Author contributions (Following the CRediT format)

Conceptualization: FZ, AM, MR, JL, EK

Methodology: FZ, AM, MR, JL, EK

Formal analysis: FZ, AM, MR, JL, EK

Investigation: all authors

Validation: all authors

Visualization: FZ, MR, JL, EK

Resources: MR

Data Curation: FZ, MR, JL, EK

Writing - Original draft: all authors

Project administration: FZ

Data availability

A GFZ Data publication (Zwaan et al., 2024), including videos of all models, is stored in this Nextcloud folder, and will be made publicly available (including a permanent DOI) on GFZ Data services (https://dataservices.gfz-potsdam.de/portal/).

- Temporary link to Nextcloud folder containing the data publication materials: https://nextcloud.gfz-potsdam.de/s/F2REjcataXFnWTb

Appendix

Model scaling procedures serve to ensure that the model adequately represents the situation in nature. Since brittle materials have time-independent rheology, the main scaling concern is the internal friction angle of the sand in our models (35˚), which is falls well in the ranges of values observed in natural upper crustal rocks (31–38˚; Byerlee, 1978; Table A1). Yet when scaling viscous materials representing the ductile lower crust, one needs to take into account their time-dependent rheology. We start with the basis equation describing the stress ratio between model and nature $\sigma*$:

$\sigma* = \rho* \cdot h* \cdot g*$ (eq. A1),

Where $\rho*$ is the density ratio, $h*$ the length ratio, and $g*$ the gravity ratio between model an nature (Hubbert 1937, Ramberg 1981). We can subsequently compute the strain rate ratio $\dot{\varepsilon}*$ from the stress ratio $\sigma*$ and viscosity ratio $\eta*$:

$\dot{\varepsilon}* = \sigma* / \eta*$ (eq. A2).

With the strain rate ratio $\dot{\varepsilon}*$, we can derive the velocity rate $v*$ and time ratio $t*$:

$\dot{\varepsilon}* = v* / h* = 1 / t*$ (eq. A3)

When assuming a relatively high lower crustal viscosity of $5 \cdot 10^{21}$ in nature, which may be representative of the situation in early-stage rift systems (e.g., Buck 1991), 1 h in our models translates to ca. 3 Myr in nature. Consequently, the model divergence velocity we apply represents a plate divergence velocity of ca. 5 mm/yr in nature, which is very close to the values in the MER (e.g., Saria et al., 2014).

Moreover, we can assess the dynamic similarity between our models and nature by comparing the R_s number and the Ramberg number R_m. The R_s number represents the ratio between gravitational stress and cohesion *C* in the brittle model materials and the upper crustal layers they represent (Ramberg 1981; Mulugeta 1998):

$$R_s = \textit{gravitational stress / cohesive strength} = (\rho \cdot h \cdot g) / C \qquad \text{(eq. A4).}$$

The cohesion of 50 Pa in our sand, combined with an assumed cohesion of 50 MPa in natural rocks (e.g., Schellart 2000, and references therein) yields an Rs value of 10 in both model and nature.

The Ramberg number is relevant to the dynamic similarity of the viscous model materials with respect to their ductile equivalents in nature, and assesses the ratio between gravitational stress and viscous strength (Weijermars & Schmeling 1986):

$$R_m = \textit{gravitational stress / viscous strength} = (\rho \cdot g \cdot h^2) / (\eta \cdot v) \qquad \text{(eq. A5)}$$

Following our calculations, the R_m number is 1.9 in both models and nature. Given that both the R_s and R_m model values are similar to those for the natural equivalent, we can consider our models properly scaled for the simulation of early-stage rifting, such as in the MER. All relevant scaling parameters used in this study are provided in Table A1.

Table A1. Scaling parameters

		Model	Nature
General parameters	Gravitational acceleration (g)	9.81 m/s^2	9.81 m/s^2
	Extension velocity (v)	$5.6 \cdot 10^{-5}$ m/s	$1.6 \cdot 10^{-10}$ m/s
Brittle layer	Material	Quartz sand	Upper crust
	Peak internal friction angle (φ_{peak})	35˚	30-38˚
	Thickness (h)	$3 \cdot 10^{-2}$ m	$2.25 \cdot 10^{4}$ m
	Density (ρ)	1700 kg/m^3	2800 kg/m^3
	Cohesion (C)	50 Pa	$50 \cdot 10^{7}$ Pa
Viscous/ ductile layer	Material	PDMS/corundum sand mix	Lower crust
	Thickness (h)	$1 \cdot 10^{-2}$ m	$7.5 \cdot 10^{4}$ m
	Density (ρ)	1600 kg/m^3	2900 kg/m^3
	Viscosity (η)	$1.5 \cdot 10^{5}$ Pa·s	$5 \cdot 10^{21}$ Pa·s
Dynamic scaling values	Brittle stress ratio (R_s)	10	10
	Ramberg number (R_m)	1.9	1.9

References

Abbate, E. and Sagri, M. (1980). Volcanites of Ethiopian and Somali Plateaus and major tectonic lines. *Atti Convegni Acc Lincei Roma, 47*, 219–227.

Abebe, T., Mazzarini, F., Innocenti, F., Manetti, P. (1998). The Yerer-Tullu Wellel volcanotectonic lineament: a transtensional structure in central Ethiopia and the associated magmatic activity. *Journal of African Earth Sciences, 26*(1), 135-150. https://doi.org/10.1016/S0899-5362(97)00141-3

Abebe Adhana, T. (2014). The occurrence of a complete continental rift type of volcanic rocks suite along the Yerer–Tullu Wellel Volcano Tectonic Lineament, Central Ethiopia. *Journal of African Earth Sciences, 99*, 374-385. https://doi.org/10.1016/j.jafrearsci.2014.02.008

Adam, J., Urai, J. L., Wieneke, B., Oncken, O., Pfeiffer, K., Kukowski, N., Lohrmann, J., Hoth, S., Van der Zee, W. and Schmatz, J. (2005). Shear localisation and strain distribution during tectonic faulting—new insights from granular-flow experiments and high-resolution optical image correlation techniques. *Journal of Structural Geology, 27*, 283-301. https://doi.org/10.1016/j.jsg.2004.08.008

Agostini, A. A., Corti, G., Zeoli, A. and Mulugeta, G. (2009). Evolution, pattern, and partitioning of deformation during oblique continental rifting: Inferences from lithospheric-scale centrifuge models. *Geochemisty, Geophysics, Geosystems, 10*, Q11015. https://doi.org/10.1029/2009GC002676

Agostini, A., Bonini, M., Corti, G., Sani, F. and Mazzarini, F. (2011). Fault architecture in the Main Ethiopian Rift and comparison with experimental models: Implications for rift evolution and Nubia–Somalia kinematics. *Earth and Planetary Science Letters, 301*, 479-492. https://doi.org/10.1016/j.epsl.2010.11.024

Bastow, I. D., A. A. Nyblade, G. W. Stuart, T. O. Rooney, and M. H. Benoit (2008), Upper mantle seismic structure beneath the Ethiopian hot spot: Rifting at the edge of the African low-velocity anomaly. *Geochemisty, Geophysics, Geosystems 9*, Q12022. https://doi.org/10.1029/2008GC002107

Bonini, M., Souriot, T., Boccaletti, M. and Brun, J. P. (1997). Successive orthogonal and oblique extension episodes in a rift zone: Laboratory experiments with application to the Ethiopian Rift. *Tectonics, 6*(2), 347–362. https://doi.org/10.1029/96TC03935

Bonini, M., Corti, G., Innocenti, F., Manetti, P., Mazzarini, F., Abebe, T. and Pecskay, Z. (2005). Evolution of the Main Ethiopian Rift in the frame of Afar and Kenya rifts propagation. *Tectonics*, *24*, TC1007. https://doi.org/10.1029/2004TC001680

Bonini, L., Fracassi, U., Bertone, N., Maesano, F. E., Valensise, G. and Basili, R. (2023). How do inherited dip-slip faults affect the development of new extensional faults? Insights from wet clay analog models. *Journal of Structural Geology, 169*, 104836. https://doi.org/10.1016/j.jsg.2023.104836

Brun, J. -P. and Tron, V. (1993). Development of the North Viking Graben: inferences from laboratory modelling. *Sedimentary Geology, 86*(1–2), 31-51. https://doi.org/10.1016/0037-0738(93)90132-O

Brune, S., Williams, S. E. and Müller, R. D. (2018). Oblique rifting: the rule, not the exception. Solid Earth, 9, 1187–1206. https://doi.org/10.5194/se-9-1187-2018

Buck, W. R. (1991). Modes of continental lithospheric extension. *Journal of Geophysical Research: Solid Earth, 96*(B12), 20161-20178. https://doi.org/10.1029/91JB01485

Byerlee, J. (1978). Friction of rocks. *Pure and Applied Geophysics, 116*, 615–626. https://doi.org/10.1007/BF00876528

Corti, G. (2008). Control of rift obliquity on the evolution and segmentation of the main Ethiopian rift. Control of rift obliquity on the evolution and segmentation of the main Ethiopian rift. Nature Geoscience, 1, 258–262. https://doi.org/10.1038/ngeo160

Corti, G. (2009). Continental rift evolution: From rift initiation to incipient break-up in the Main Ethiopian Rift, East Africa. *Earth-Science Reviews, 96*(1–2), 1-53. https://doi.org/10.1016/j.earscirev.2009.06.005

Corti, G., Sani, F., Agostini, S., Philippon, M., Sokoutis, D. and Willingshofer, E. (2018). Off-axis volcano-tectonic activity during continental rifting: Insights from the transversal Goba-Bonga lineament, Main Ethiopian Rift (East Africa). *Tectonophysics, 728–729*, 75-91. https://doi.org/10.1016/j.tecto.2018.02.011

Corti, G., Maestrelli, D. and Sani, F. (2022). Large-to Local-Scale Control of Pre-Existing Structures on Continental Rifting: Examples From the Main Ethiopian Rift, East Africa. Frontiers in Earth Science, 10, 808503. https://doi.org/10.3389/feart.2022.808503

DeMets, C. and Merkouriev, S. (2016). High-resolution estimates of Nubia–Somalia plate motion since 20 Ma from reconstructions of the Southwest Indian Ridge, Red Sea and Gulf of Aden. *Geophysical Journal International, 207*(1), 317–332. https://doi.org/10.1093/gji/ggw276

DeMets, C. and Merkouriev, S. (2021). Detailed reconstructions of India–Somalia Plate motion, 60 Ma to present: implications for Somalia Plate absolute motion and India–Eurasia Plate motion. *Geophysical Journal International, 227*, 1730-1767. https://doi.org/10.1093/gji/ggab295

Erbollo, A., Corti, G., Agostini, A., Sani, Kidane, T. and Buccanti, A. (2016). Modeling along-axis variations in fault architecture in the Main Ethiopian Rift: Implications for Nubia-Somalia kinematics. *Journal of Geodynamics, 102*, 24-38. https://doi.org/10.1016/j.jog.2016.07.002v

Hayward, N. J. and Ebinger, C. J. (1996). Variations in the along-axis segmentation of the Afar Rift system. *Tectonics, 15*(2), 244-257. https://doi.org/10.1029/95TC02292

Henza, A., A., Withjack, M. O. and Schlische, R. (2010). Normal-fault development during two phases of non-coaxial extension: An experimental study. Journal of Structural Geology, 32(11), 1656-1667. https://doi.org/10.1016/j.jsg.2009.07.007

Henza, A., A., Withjack, M. O. and Schlische, R. (2010). How do the properties of a pre-existing normal-fault population influence fault development during a subsequent phase of extension? Journal of Structural Geology, 33(9), 1312-1324. https://doi.org/10.1016/j.jsg.2011.06.010

Keep, M. and McClay, K. R. (1997). Analogue modelling of multiphase rift systems. *Tectonophysics, 273*(3–4), 239-270. https://doi.org/10.1016/S0040-1951(96)00272-7

Keir, D., Ebinger, C. J., Stuart, G. W., Daly, E. and Ayele, A. (2006). Strain accommodation by magmatism and faulting as rifting proceeds to breakup: Seismicity of the northern Ethiopian rift. Journal of Geophysical Research: Solid Earth, 111, B05314. https://doi.org/10.1029/2005JB003748

Keir, D., Hamling, I. J., Ayele, A., Ebinger, C., Wright, T. J., Jacques, E., Mohamed, K., Hammond, J. O. S., Belachew, M., Baker, E., Rowland, J. V., Lewi., E. and Bennati, L. (2009). Evidence for focused magmatic accretion at segment centers from lateral dike injections captured beneath the Red Sea rift in Afar. Geology, 37(1), 59-62. https://doi.org/10.1130/G25147A.1

Keranen, K. and Klemperer, S. L. (2008). Discontinuous and Diachronous Evolution of the Main Ethiopian Rift: Implications for the Development of continental Rifts. *Earth and Planetary Science Letters*, *265*, 96–111. https://doi.org/10.1016/j.epsl.2007.09.038

Keranen, K., Klemperer, S. L., Julia, J., Lawrence, J. F. and Nyblade, A. A. (2009). Low lower crustal velocity across Ethiopia: Is the Main Ethiopian Rift a narrow rift in a hot craton? *Geoschemisty, Geophysics, Geosystems, 10*, Q0AB0. https://doi.org/10.1029/2008GC002293

Knappe, E., Bendick, R., Ebinger, C., Birhanu, Y., Lewi, E., Floyd, M., Kind, R., Kianji, G., Mariita, N., Temtime, T., Waktola, B., Deresse, B., Musila, M., Kanoti, J., and Perry, M. (2020). Accommodation of East African Rifting across the Turkana Depression. *Journal of Geophysical Research: Solid Earth, 125*, e2019JB018469. https://doi.org/10.1029/2019JB018469

Korme, T., Acocella, V. and Abebe, B. (2004). The Role of Pre-existing Structures in the Origin, Propagation and Architecture of Faults in the Main Ethiopian Rift. *Gondwana Research*, *7*(2), 467-479. https://doi.org/10.1016/S1342-937X(05)70798-X

Le Calvez, J. H. and Vendeville, B. (2002). Experimental designs to model along-strike fault interactions.

Maestrelli, D., Sani, F., Keir, D., Pagli, C., La Rosa, A., Muluneh, A. A., Brune, S. and Corti, G. (2024). Reconciling plate motion and faulting at a rift-rift-rift triple junction. *Geology, 52*(5), 362-266. https://doi.org/10.1130/G51909.1

Merla, G., Abbate, E., Azzaroli, A., Bruni, P., Canuti, P., Fazzuoli, M., Sagri, M. and Tacconi, P. (1979). A geological map of Ethiopia and Somalia at 1/2.000.000, and comment with a map of major landforms https://www.sidalc.net/search/Record/unfao:668634/Description https://doi.org/10.1016/0012-8252(80)90110-5

Michon, L. and Merle, O. (2000). Crustal structures of the Rhinegraben and the Massif Central grabens: An experimental approach. *Tectonics*, *19*(5), 896-904. https://doi.org/10.1029/2000TC900015

Michon, L., Famin, V. and Quidelleur, X. (2022). Evolution of the East African Rift System from trap-scale to plate-scale rifting. *Earth-Science Reviews, 231*, 104089. https://doi.org/10.1016/j.earscirev.2022.104089

Molnar, N. E., Cruden, A. R. and Betts, P. G. (2019). Interactions between propagating rifts and linear weaknesses in the lower crust. *Geosphere, 15*(5), 1617-1640. https://doi.org/10.1130/GES02119.1

Molnar, N., Cruden. A. and Betts, P. (2020). The role of inherited crustal and lithospheric architecture during the evolution of the Red Sea: Insights from three dimensional analogue experiments. *Earth and Planetary Science Letters, 544*, 116377. https://doi.org/10.1016/j.epsl.2020.116377

Mulugeta, B. (1988). Squeeze box in a centrifuge. *Tectonophysics, 148*(3–4), 323-335. https://doi.org/10.1016/0040-1951(88)90139-4

Muhabaw, Y., Muluneh, A. A., Nugsse, K., Gebru, E. F. and Kidane, T. (2022). Paleomagnetism of Gedemsa magmatic segment, Main Ethiopian Rift: Implication for clockwise rotation of the segment in the Early Pleistocene. Tectonophysics, 838, 229475. https://doi.org/10.1016/j.tecto.2022.229475

Muluneh, A. A., Brune, S., Illsley-Kemp, F., Corti, G., Keir, D., Glerum, A., Kidane, T. and Mori, J. (2020). Mechanism for Deep Crustal Seismicity: Insight From Modeling of Deformation Processes at the Main Ethiopian Rift. *Geochemisty, Geophysics, Geosystems, 21*(7), e2020GC008935. https://doi.org/10.1029/2020GC008935

Osagiede, E. E., Rosenau, M., Rotevatn, A., Gawthorpe, R., Jackson, C. A. -L. and Rudolf, M. (2021). Influence of Zones of Pre-Existing Crustal Weakness on Strain Localization and Partitioning During Rifting: Insights From Analog Modeling Using High-Resolution 3D Digital Image Correlation. *Tectonics, 40*(10), e2021TC006970. https://doi.org/10.1029/2021TC006970

Rosenau, M., Pohlenz, A., Kemnitz, H. and Warsitzka, M. (2018). Ring-shear test data of quartz sand G12 used for analogue experiments in the Helmholtz Laboratory for Tectonic Modelling (HelTec) at the GFZ German Research Centre for Geosciences in Potsdam. *GFZ Data Services*. https://doi.org/10.5880/GFZ.4.1.2019.003

Rosenau, M. and Pohlenz, A. (2023). Ring-shear test data of corundum sand “NKF120” used for analogue modelling in the experimental tectonics laboratory at GFZ Potsdam. *GFZ Data Services*. https://doi.org/10.5880/GFZ.4.1.2023.009

Rudolf, M., Boutelier, D., Rosenau, M., Schreurs, G. and Oncken, O. (2016). Rheological benchmark of silicone oils used for analog modeling of short- and long-term lithospheric deformation. *Tectonophysics, 684*, 12-22. https://doi.org/10.1016/j.tecto.2015.11.028

Saria, E., Calais, E., Stamps, D. S., Delvaux, D. and Hartnady, C. J. H. (2014). Present-day kinematics of the East African Rift. *Journal of Geophysical Research: Solid Earth, 119*(4), 3584-3600. https://doi.org/10.1002/2013JB010901

Stamps, D. S., Kreemer, C., Fernandes, R., Rajaonarison, T. A. and Rambolamanana, G. (2021). Redefining East African Rift System kinematics, *Geology, 49*(2), 150-155. https://doi.org/10.1130/G47985.1

Tomassini, S., Manetti, P., Innocenti, F., Abebe, T., Sintoni, M. and Conticelli, S. (2005). The Ethiopian subcontinental mantle domains: geochemical evidence from Cenozoic mafic lavas. *Mineralogy and Petrology*, 84, 259-281. https://doi.org/10.1007/s00710-005-0081-9

Tron, V. and Brun, J. -P. (1991). Experiments on oblique rifting in brittle-ductile systems. Tectonophysics 188, (1–2), 71-84. https://doi.org/10.1016/0040-1951(91)90315-J

Wang, L., Maestrelli, D., Corti, G., Zou, Y. and Shen, C. (2021). Normal fault reactivation during multiphase extension: Analogue models and application to the Turkana depression, East Africa. Tectonophysics 811, 228870. https://doi.org/10.1016/j.tecto.2021.228870

Weijermars, R. and Schmeling, H. (1986). Scaling of Newtonian and non-Newtonian fluid dynamics without inertia for quantitative modelling of rock flow due to gravity (including the concept of rheological similarity). *Physics of the Earth and Planetary Interiors, 43*(4), 316-330. https://doi.org/10.1016/0031-9201(86)90021-X

Withjack, M. O. and Jamison, W. R. (1986). Deformation produced by oblique rifting. Tectonophysics, 126, (2–4), 99-124. https://doi.org/10.1016/0040-1951(86)90222-2

Zou, Y., Maestrelli, D., Corti, G., Del Ventisette, C., Wang, L., and Shen, C. (2024). Influence of inherited brittle fabrics on continental rifting: Insights from centrifuge experimental modeling and application to the East African Rift System. *Tectonics, 43*, e2023TC007947. https://doi.org/10.1029/2023TC007947

Zwaan, F. and Schreurs, G. (2017). How oblique extension and structural inheritance influence rift segment interaction: Insights from 4D analog models. *Interpretation, 5*(1), 1F-T141. https://doi.org/10.1190/INT-2016-0063.1

Zwaan, F., Schreurs, G. and Adam, J. (2018). Effects of sedimentation on rift segment evolution and rift interaction in orthogonal and oblique extensional settings: Insights from analogue models analysed with 4D X-ray computed tomography and digital volume correlation techniques. *Global and Planetary Change, 171*, 110-133. https://doi.org/10.1016/j.gloplacha.2017.11.002

Zwaan, F., Schreurs, G., Ritter, M., Santimano, T. and Rosenau, M. (2018). Rheology of PDMS-corundum sand mixtures from the Tectonic Modelling Lab of the University of Bern (CH). V. 1. *GFZ Data Services*. https://doi.org/10.5880/fidgeo.2018.023

Zwaan, F., Schreurs, G. and Buiter, S.J.H. (2019). A systematic comparison of experimental set-ups for modelling extensional tectonics. *Solid Earth, 10*(4), 1063-1097. https://doi.org/10.5194/se-10-1063-2019

Zwaan, F., Chenin, P., Erratt, D., Manatschal, G. and Schreurs, G. (2021). Complex rift patterns, a result of interacting crustal and mantle weaknesses, or multiphase rifting? Insights from analogue models. *Solid Earth, 12*(7), 1473-1495. https://doi.org/10.5194/se-12-1473-2021

Zwaan, F., Chenin, P., Erratt, D., Manatschal, G. and Schreurs, G. (2022). Competition between 3D structural inheritance and kinematics during rifting: Insights from analogue models. *Basin Research, 34*(2), 824-854. https://doi.org/10.1111/bre.12642

Zwaan, F., Muluneh, A. A., Liu, J., Kosari, E., Rosenau, M., Corti, G. and Sani, F. (2024). Results of analogue tectonic models of rifting and tectonic lineament reactivation in the Main Ethiopian Rift. *GFZ Data Services.*

- Temporary link to Nextcloud folder containing the data publication materials : https://nextcloud.gfz-potsdam.de/s/F2REjcataXFnWTb